Coke and Sintering Resistant Nickel Atomically Doped Ceria Nanosheets for Highly Efficient Solar Driven Hydrogen Production from Bioethanol

Dachao Yuan,‡*[a] Yahang Peng,‡[a] Luping Ma,‡[a] Jianchang Li,[a] Jianguo Zhao,[a] Jianjun Hao,*[a] Shufang Wang,[a,b] Baolai Liang,[b] Jinhua Ye,[c] Yaguang Li*[a,b]

[a] *College of Mechanical and Electrical Engineering, Key Laboratory Intelligent Equipment and New Energy Utilization of Livestock and Poultry Breeding, Hebei Agricultural University, Baoding 071001, China. E-mail: jdydch@hebau.edu.cn, hjjpaper@163.com.*

[b] *Hebei Key Lab of Optic-electronic Information and Materials, The College of Physics Science and Technology, Institute of Life Science and Green Development, Hebei University, Baoding, 071002, China. E-mail: liyaguang@hbu.edu.cn.*

[c] *International Center for Materials Nanoarchitectonics (WPI-MANA), National Institute for Materials Science (NIMS), 1-1 Namiki, Tsukuba, Ibaraki 305-0044, Japan.*

Electronic Supplementary Information (ESI) available: details of any supplementary information available should be included here. See DOI: 10.1039/x0xx00000x

‡These authors contributed equally.

Experimental Section

Chemicals

$Ni(NO_3)_2 \cdot 6H_2O$, HNO_3, $C_2H_8N_2$ and $NH_3 \cdot H_2O$ were purchased from Tianjin Damao Chemical Reagent Co., Ltd., $Ce(NO_3)_3 \cdot 6H_2O$ were purchased from Tianjin Kermel Chemical Reagent Co., Ltd., Citric acid was purchased from Tianjin Beichen Founder Reagent Factory, ethanol was purchased from Beilian chemical industry Co., Ltd. All chemicals were directly used without further treatment. The mixture of water and bioethanol used for ESR was in the ratio of 13:1, which was referred to the ratio of corn fermentation broth.

Catalysts preparation

Ni SA/CeO_2

The Ni SA/CeO_2 was prepared by followed procedures. Firstly, 5 g citric acid was measured as the complexing agent, 0.2 g $Ni(NO_3)_2 \cdot 6H_2O$ and 2 g $Ce(NO_3)_3 \cdot 6H_2O$ were all dissolved in 10 mL of deionized water and stirred for 10 min. Then, 2.5 mL nitric acid and 1 mL ethylenediamine were added as the viscosity agent. After fully stirring, ammonia was added to adjust the pH value to about 6. Subsequently, the solution was stirred and dried at 80 ℃, and then moved to a 100 ℃ constant temperature drying oven for 24 h. The product was calcined in argon at 400 °C for 3 h to get the expanded solid and then calcinated in the air at 400 °C for 4 h to prepare the Ni SA/CeO_2 (the Ni/Ce atomic ratios were 0.15).

Ni P/CeO_2

The synthesis of Ni P/CeO_2 was similar to that of Ni SA/CeO_2 and the only difference was that the mass of $Ni(NO_3)_2 \cdot 6H_2O$ was 0.5 g. By varying the amount of Ni, the Ni/Ce atomic ratio was tuned to 0.375. To increase the ESR activity, the Ni P/CeO_2 nanosheets were annealed under 10% H_2/Ar at 400 °C for 3 h (Figure S8).

We used ICP-AES to test the actual atomic ratio of Ni in Ni SA/CeO_2 and Ni P/CeO_2. The Ni/Ce ratio was estimated to be 15.03 at.%, 37.45 at.% in Ni SA/CeO_2 and Ni P/CeO_2, respectively.

CeO_2

The synthesis of CeO_2 nanosheets was similar to that of Ni SA/CeO_2 and the only difference was the absence of $Ni(NO_3)_2 \cdot 6H_2O$.

Thermal catalytic test

The thermal ESR catalytic activity of catalysts was tested by the fixed-bed reactor (XM190708-007, DALIAN ZHONGJIARUILIN LIQUID TECHNOLOGY CO., LTD) in continuous flow form. Typically, 10 mg catalyst was placed in a quartz flow reactor. 50 sccm Ar was regulated by a mass flow controller and the steam generated by the raw water and ethanol (molar ratio of 13:1) heated in a water bath at 80 ℃ was introduced into the reaction system to start the reaction. The product first passed through a condenser to condense the unreacted ethanol and water, and then the gas entered a gas chromatograph (GC) 7890A for analysis. In the gas chromatograph, the gas first passed through the TCD detector to detect H_2, and then passed through the FID detector to detect CO, CH_4 and CO_2.

The TOF calculation was as follows:

$$TOF_{Ni\ SA/CeO2}\ (h^{-1}) = (Q_{Ni\ SA/CeO2}-Q_{CeO2})/M_{Ni\ SA/CeO2} \quad (1)$$

$$TOF_{Ni\ P/CeO2}\ (h^{-1}) = (Q_{Ni\ P/CeO2}-Q_{CeO2})/M_{Ni\ P/CeO2} \quad (2)$$

$Q_{Ni\ SA/CeO2}$, $Q_{Ni\ P/CeO2}$, Q_{CeO2} was the ESR hydrogen flow rate (mol h^{-1}) of Ni SA/CeO_2, Ni P/CeO_2, CeO_2, respectively. $M_{Ni\ SA/CeO2}$, $M_{Ni\ P/CeO2}$ was the molar amount of Ni in Ni SA/CeO_2, Ni P/CeO_2, respectively.

Sunlight driven ESR

The laboratory light source we used for the test was a customized product (HP-2-4000, provided by Hebei scientist research experimental and equipment trade Co., Ltd.). 3 g of catalysts were loaded in the solar heating device (irradiation area ~500 cm^2) irradiated by HP-2-4000. A raw material containing water and bioethanol (molar ratio of 13:1) was pumped into the system. A flowmeter (MV-192-H2, Bronkhorst) was used to measure the flow rate of

produced gases. The outlet gases were tested by gas chromatograph (GC) 7890A equipped with FID and TCD detectors.

The solar heating device was similar to that in our previous report,[1] except that the selective light absorber was changed by Ti_2O_3 and the Al film was replaced by Cu film.

The hydrogen generation rate of the catalyst (δ, mmol g^{-1} h^{-1}) from the solar heating system was calculated as follows:

δ (mmol g^{-1} h^{-1}) = (1000*L/24.5)/G (3)

L was the hydrogen flow rate (L h^{-1}), G was the weight of catalysts (3 g).

Outdoor sunlight driven ESR

The outdoor sunlight driven ESR was similar to the sunlight driven ESR. The only difference was that a parabolic reflector (with 0.5 m^2 of reflection area) was used to concentrate the sparse outdoor sunlight on the solar heating device. The install of the parabolic reflector was based on the ecliptic plane. The gases flow rate was tested by a flowmeter (C50 5SLM) and the outdoor sunlight driven ESR was operated from 10:00 to 14:00 on December 14, 2021, in Baoding, China.

Enthalpy change energy of chemicals

The enthalpy change energy of ethanol (l), CO_2 (g), H_2 (g), H_2O (l) was -276.981, -393.505, 0, -285.830 kJ mol^{-1}, respectively.

The (g) and (l) indicated the gas state and liquid state, respectively.

STH calculation

The STH efficiency of hydrogen generation from ESR was calculated as follows:

STH= (ΔH*ε/24.5)/(I*S*3600) (4)

ΔH was the reaction enthalpy change of ethanol dehydrogenation (1/6 C_2H_5OH (l) + 1/2 H_2O (l)→ H_2 (g)+ 1/3 CO_2 (g), ΔH=57.91 kJ mol^{-1}), ε (L) was the H_2 generation amount per hour detected by a flowmeter (MV-192-H2), I was the light intensity (kW m^{-2}), S was the irradiated

area of catalysts (0.05 m^{-2}). There was a small amount of CO and CH_4 that existed in the produced gas, which were ignored in this calculation, considering their small amount.

Characterizations

The overall composition of the prepared samples was studied by the powder X-ray diffraction (XRD), which was performed on a Bede D1 system operated at 20 kV and 30 mA with Cu Kα radiation (λ= 1.5406 Å). ARM 200 F and JEOL F200+ were used to identify the morphology and the crystal structure of the nanostructures. Zennium_Pro (Zahner, Germany) was an electrochemical workstation. N_2-sorption isotherms were collected on a Belsorb-Max system. Brunauer-Emmett-Teller (BET) specific surface areas were calculated from the adsorption data. Platinum resistance thermometer (M363886) was used for detecting the data of temperatures. Thermo ESCALAB-250 spectrometer with a monochromatic Al Kα radiation source (1486.6 eV) was used to detect the valence state of materials. Raman spectra were recorded on a HORIBA Raman spectrometer, with an excitation laser wavelength of 532 nm. The FTIR was tested by HYPERION 3000 (Bruker Optics). The thickness of catalysts was tested by AFM (MFP-3D Origin+, Oxford Instruments). The ICP-AES was tested by Thermo ICAP 6300 and the catalysts were dissolved by 4 M HNO_3 at 150 °C for 6 h.

EXAFS test and analysis.

The Ni K-edge and Ce K-edge extended X-ray absorption fine structure (EXAFS) data were collected on the beamline at Shanghai Synchrotron Radiation Facility (SSRF). All samples were prepared by placing a small amount of homogenized (via agate mortar and pestle) powder on 3M tape. We used IFEFFIT software to calibrate the energy scale, correct the background signal and normalize the intensity. The spectra were normalized with respect to the edge height after subtracting the pre-edge and post-edge backgrounds using Athena software. To extract the EXAFS oscillations, the background was removed in k-space using a five-domain cubic spline. The resulting k-space data were then Fourier transformed.

First principle calculation

The Vienna Ab Initio Package (VASP)[2, 3] has been used to conduct all the DFT calculations within the generalized gradient approximation (GGA) using the PBE formulation.[4] The projected augmented wave (PAW) potentials[5, 6] were chosen to describe the ionic cores and take valence electrons into account using a plane wave basis set with a kinetic energy cutoff of 400 eV. Partial occupancies of the Kohn−Sham orbitals were allowed using the Gaussian smearing method and a width of 0.05 eV. The electronic energy was considered self-consistent when the energy change was smaller than 10^{-7} eV. Geometry optimization was considered convergent when the energy change was smaller than 10^{-6} eV. Grimme's DFT-D3 methodology[7] was used to describe the dispersion interactions among all the atoms in the bulk unit cells and surface models of interest.

The equilibrium lattice constant of face-centered cubic (FCC) Ni unit cell was optimized using a 15×15×15 Monkhorst-Pack k-point grid for Brillouin zone sampling, to be a=3.476 Å. We then use it to construct a Ni (111) surface model with *p*(4x3) periodicity in the x and y directions and 4 atomic layers in the z direction by vacuum depth of 15 Å in order to separate the surface slab from its periodic duplicates. This Ni (111) surface model contains 48 atoms. During structural optimizations, the gamma point in the Brillouin zone was used for k-point sampling, and the top two atomic layers were allowed to fully relax while the bottom two were fixed.

The equilibrium lattice constant of CaF_2-type Ni SA/CeO_2 unit cell was optimized when using an 11×11×11 Monkhorst-Pack k-point grid for Brillouin zone sampling, to be a=5.479 Å. We then use it to construct a CeO_2 (111) surface model with *p*(4x3) periodicity in the x and y directions and 3 O-Ce-O tri-layers in the z direction by vacuum depth of 15 Å in order to separate the surface slab from its periodic duplicates. This CeO_2 (111) surface model contains 1 Ni, 35 Ce and 72 O atoms. During structural optimizations, the gamma point in the

Brillouin zone was used for k-point sampling, and the top one layer was allowed to fully relax while the bottom two were fixed.

Steam reforming test

The CO, CH_4 steam reforming tests were tested by the fixed-bed reactor (XM190708-007, DALIAN ZHONGJIARUILIN LIQUID TECHNOLOGY CO., LTD.) in continuous flow form. Typically, 20 mg catalyst was placed in a quartz flow reactor. The feed gas composition for CO steam reforming was (vol.) 4 % CO and 6 % H_2O balanced with Ar (the gas flow rate of CO+Ar is 100 sccm). The feed gas composition for CH_4 steam reforming was (vol.) 2 % CH_4 and 16 % H_2O balanced with Ar (the gas flow rate of CH_4+Ar is 100 sccm). The reaction products were tested by gas chromatograph (GC) 7890A equipped with FID and TCD detector.

The deposition of Ti_2O_3 film and synthesis of devices

The SP-0707AS magnetron sputtering was used to deposit Ti_2O_3 film, which had the vacuum pressure lower than 7.0×10^{-3} Pa, and a 4 axis rotation system to rotate bases. Ti_2O_3 and Cu were used as targets; the working gas was Ar with 99.99 % purity. The bases used in Figure 4b,c and Figure 4d,e,f were Cu film with 20×20×0.1 mm size and quartz reaction tube, respectively. Before the deposition process, the bases were washing with deionized water, acetone, ethanol subsequently.

1. The deposition of Ti_2O_3 film on Cu film was first using glow-discharge to clean Cu film, then depositing the Ti_2O_3 film, finally taking out the sample after passive cooling. Specific parameters: the power was 5 KW, the sputtering pressure was 9×10^{-2} Pa, the bias voltage was 150 V, the sputtering temperature was 70 °C, the sputtering time was 6 min for Ti_2O_3 film, respectively.
2. For the synthesis of Ti_2O_3/Cu based device, the deposition of Cu substrate and Ti_2O_3 film on reaction tube was first using glow-discharge to clean glass tube, then depositing Cu layer by Cu target and Ti_2O_3 film by Ti_2O_3 target orderly, finally taking out the sample

after passive cooling. Specific parameters: the power was 5 KW, the sputtering pressure was 9×10^{-2} Pa, the bias voltage was 150 V, the sputtering temperature was 70 °C, the sputtering time for Cu layer, Ti_2O_3 film was 12 min, 6 min, respectively. The followed glass vacuum layer was provided by Hebei scientist research experimental and equipment trade Co., Ltd. with 1×10^{-3} Pa of pressure.

Table S1. EXAFS fitting parameters of Ni SA/CeO_2 with NiO and Ni foil extracted from the Ni K-edge

sample	Path	CN	$\sigma^2(10^{-3}$ Å$^2)$	R	ΔE_0(eV)
Ni foil	Ni-Ni	12	5.9±0.4	2.48±0.03	7.5
NiO	Ni-O	6	7.6±0.3	1.88±0.02	-3.9
	Ni-Ni	12	7.2±1.0	2.94±0.03	-4.6
Ni SA/CeO_2	Ni-O	8.0±1.0	3.9±1.1	2.15±0.03	-5.5

The E_0 value of Ni K-edge (the first inflection point on the edge) from Ni SA/CeO_2, NiO, Ni foil was 8333 eV, 8334 eV, 8325 eV, respectively.

We took a comparative experiment of ESR driven by the electric furnace. When the hydrogen production rate was 40 L h^{-1}, the input power of the electric furnace was 84 W.

The electric energy-hydrogen energy efficiency (ETH) of ESR was calculated as follows:

$$ETH = (\Delta H * \varepsilon / 24.5) / (I * 3600) \quad (5)$$

ΔH was the reaction enthalpy change of ethanol dehydrogenation (1/6 C_2H_5OH (l) + 1/2 H_2O (l)→ H_2 (g)+ 1/3 CO_2 (g), ΔH=57.91 kJ mol^{-1}), ε (L) was the H_2 generation amount per hour (40 L h^{-1}), I was the input power of the electric furnace (0.084 kW).

The ETH was calculated to be 31.2%.

According to the solar-electric energy efficiency of monocrystalline silicon solar cells at maximum 25%,[8] the STH according to the path of solar-electric energy-thermal energy-chemical energy was calculated as 25%*31.2%=7.8%, far less than the our reported STH (16.7%) through the solar-thermal energy-chemical energy path.

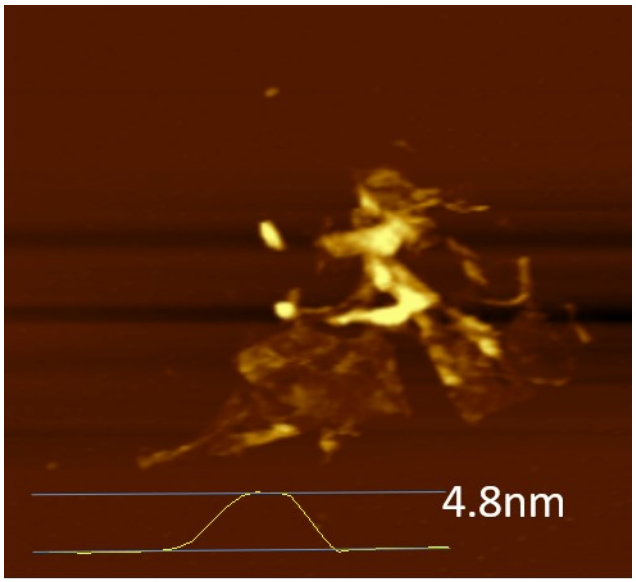

Figure S1. AFM image of Ni SA/CeO_2.

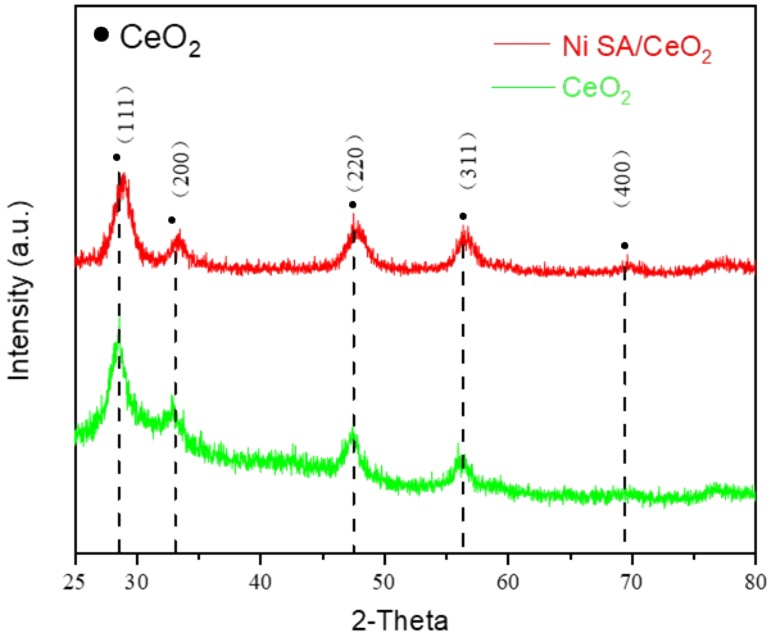

Figure S2. The XRD pattern of Ni SA/CeO_2 and CeO_2.

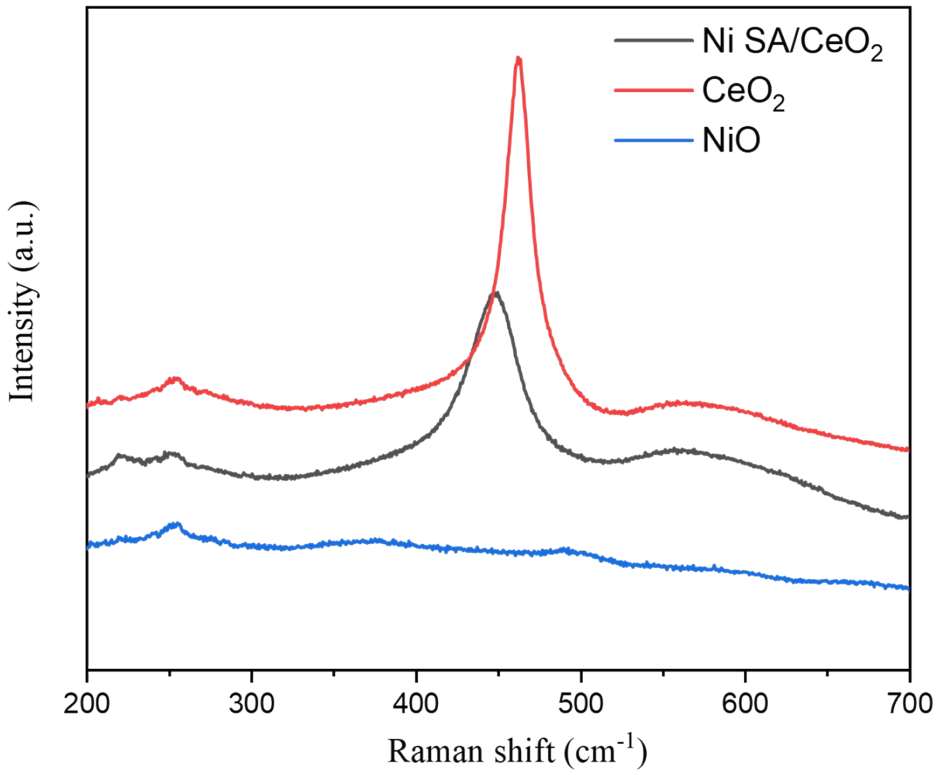

Figure S3. The Raman spectra of Ni SA/CeO_2, NiO, CeO_2.

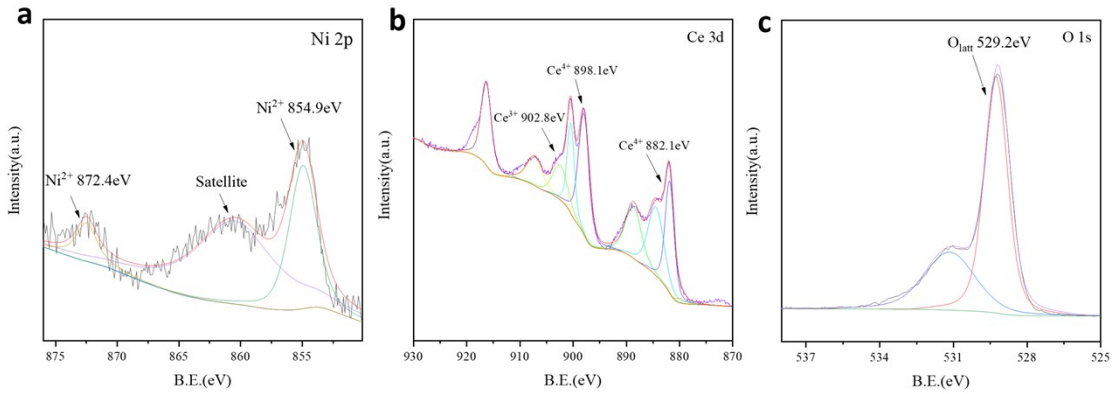

Figure S4. (a, b, c) Ni 2p, Ce 3d, O1s XPS spectra of Ni SA/CeO_2.

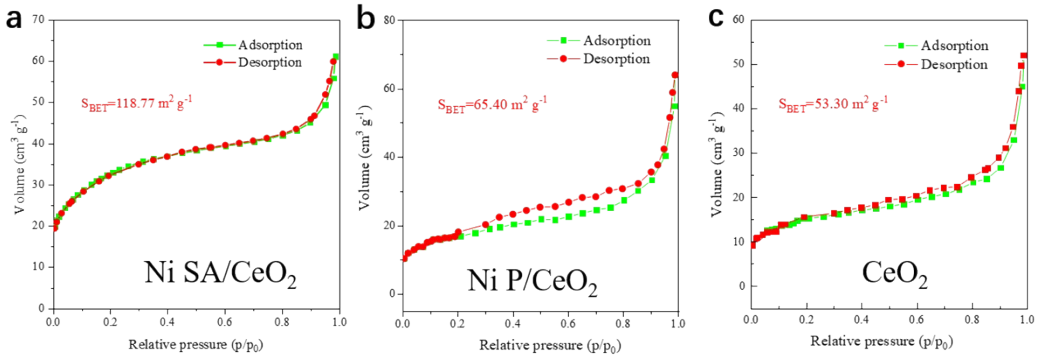

Figure S5. Nitrogen adsorption and desorption isotherms of the Ni SA/CeO_2 (a), Ni P/CeO_2 (b), CeO_2 (c).

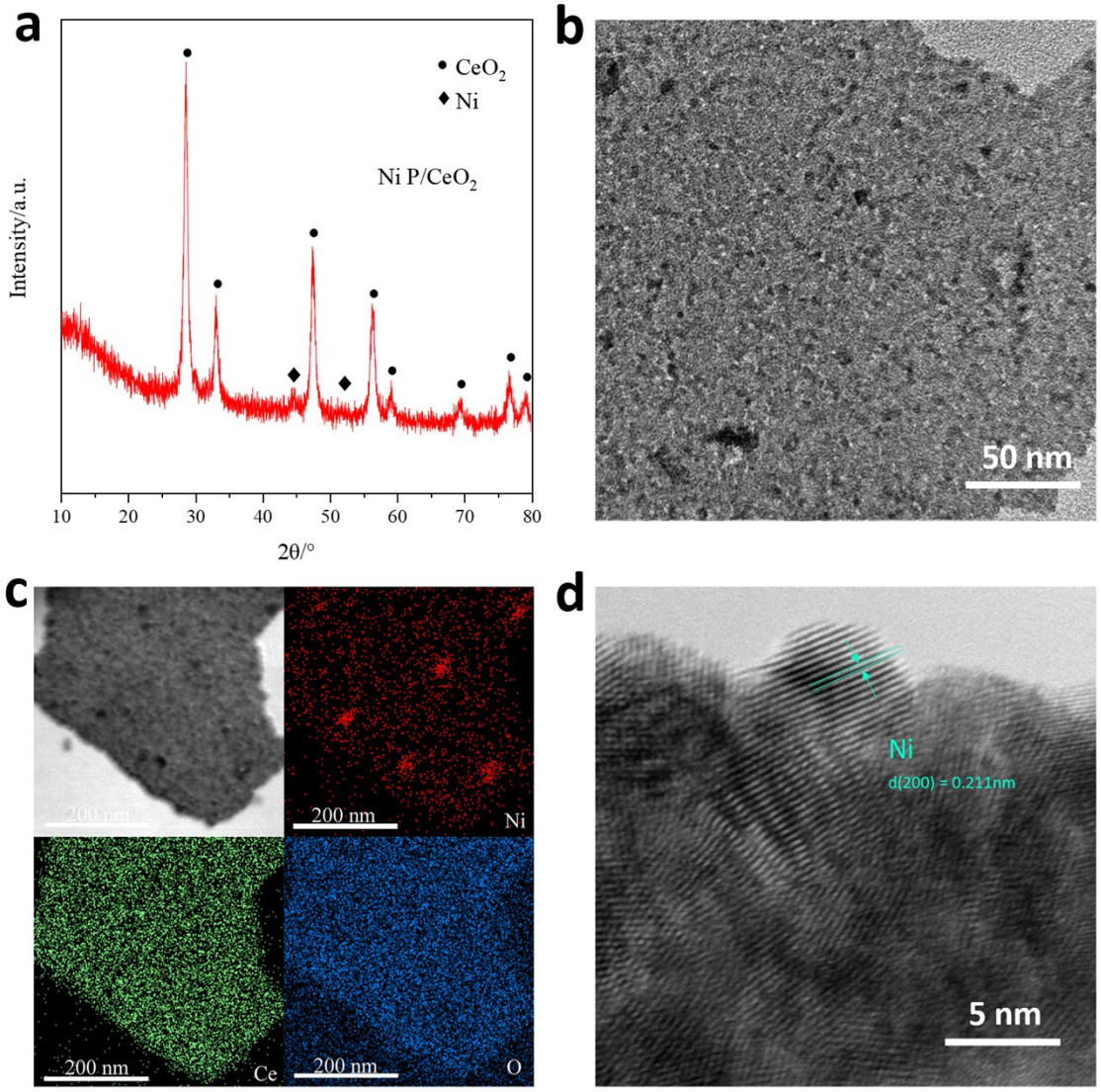

Figure S6. (a) XRD pattern, (b) TEM image, (c) STEM image and elemental mappings, (d) HRTEM image of the Ni P/CeO_2.

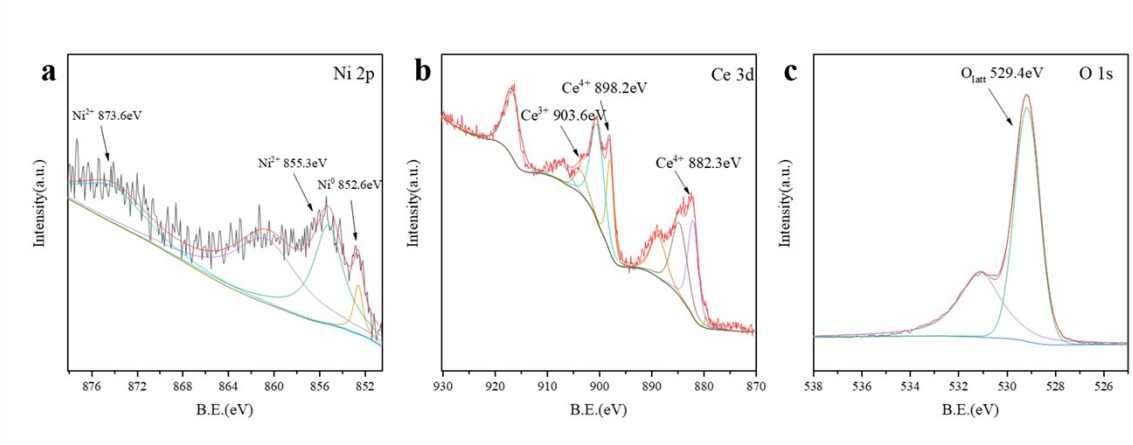

Figure S7. (a, b, c) Ni 2p, Ce 3d, O1s XPS spectra of Ni P/CeO_2.

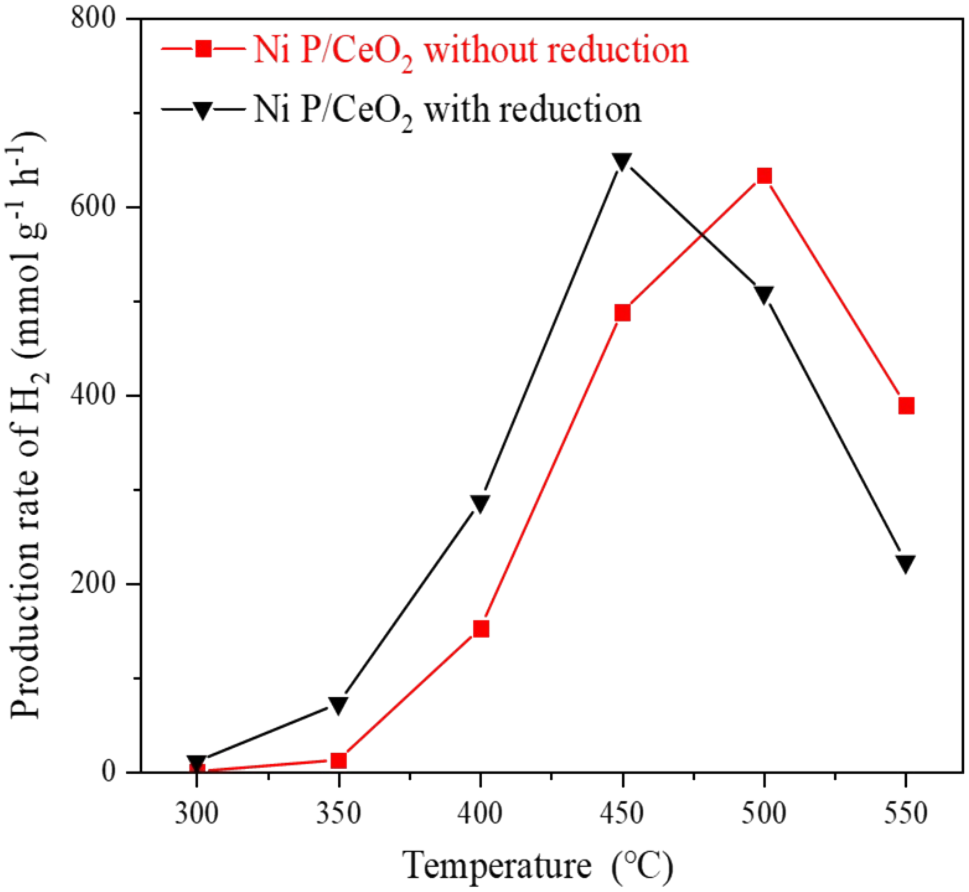

Figure S8. The hydrogen production rate of thermocatalytic ESR using the Ni P/CeO_2 with and without reduction process.

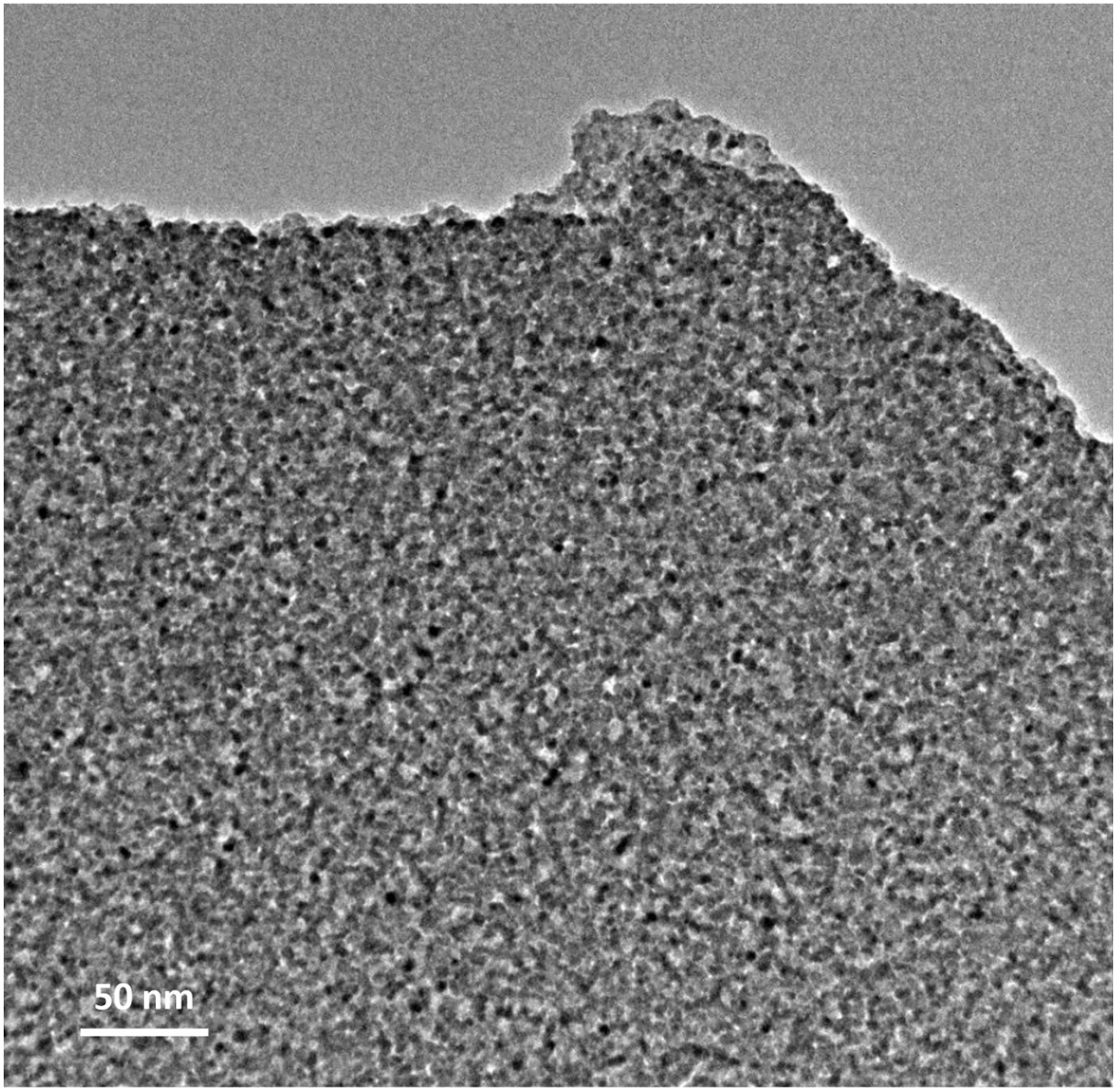

Figure S9. TEM image of the CeO_2.

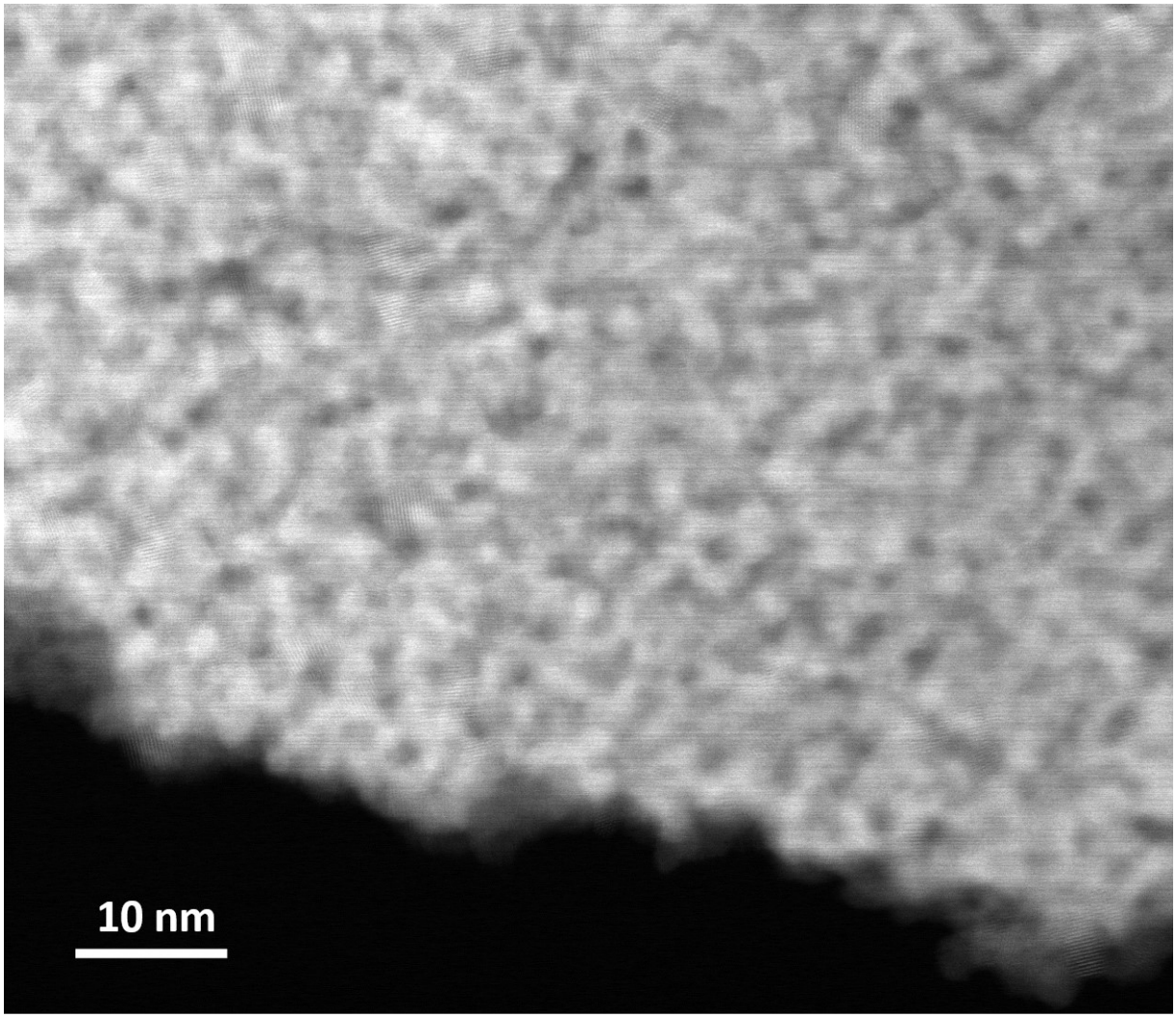

Figure S10. STEM image of Ni SA/CeO_2 after ESR stability test.

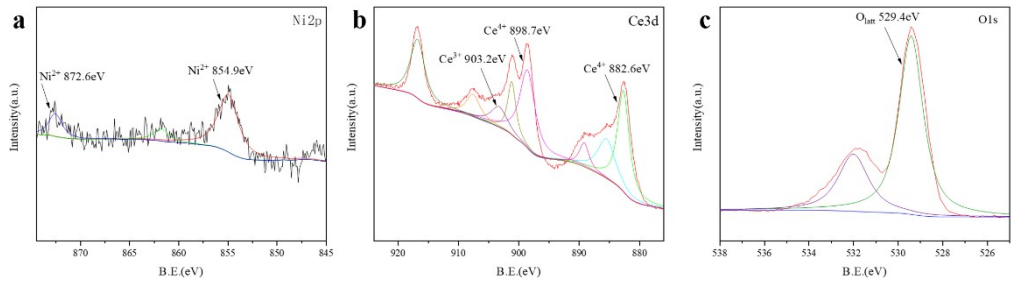

Figure S11. (a, b, c) Ni 2p, Ce 3d, O1s XPS spectra of Ni SA/CeO_2 after ESR stability test.

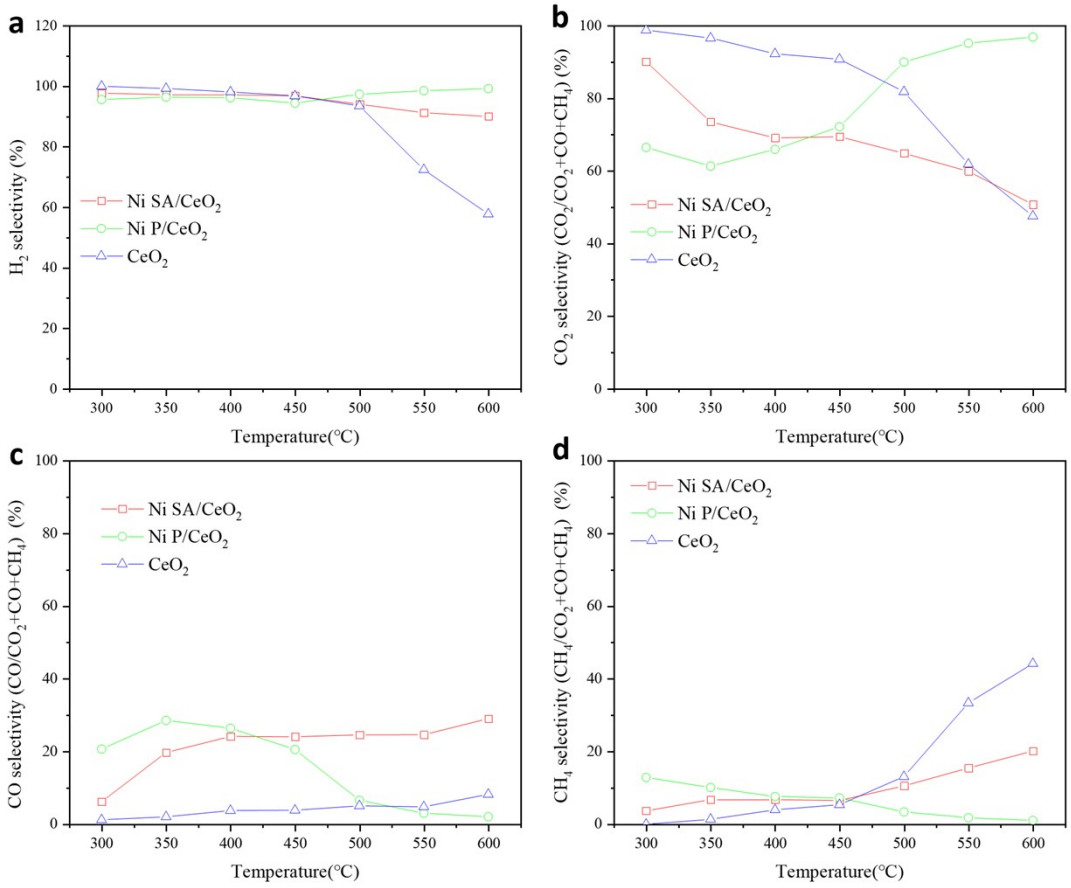

Figure S12. (a) H_2 selectivity of Ni SA/CeO_2, Ni P/CeO_2, CeO_2 as a function of temperature. (b) CO_2 selectivity of Ni SA/CeO_2, Ni P/CeO_2, CeO_2 as a function of temperature. (c) CO selectivity of Ni SA/CeO_2, Ni P/CeO_2, CeO_2 as a function of temperature. (d) CH_4 selectivity of Ni SA/CeO_2, Ni P/CeO_2, CeO_2 as a function of temperature.

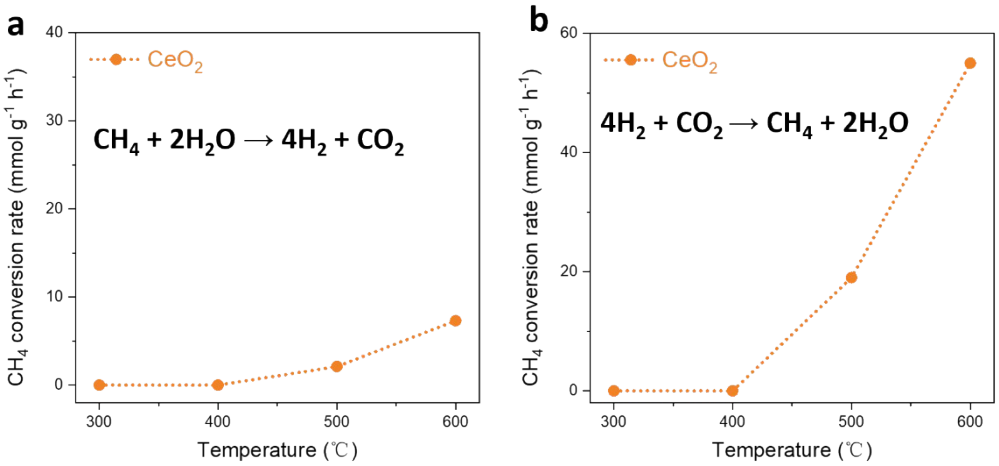

Figure S13. (a, b) The CH_4 steam reforming and CO_2 methanation performance over CeO_2.

Through the experiments, we found that CeO_2 had a low activity for CH_4 reforming and a relative high activity for CO_2 methanation at high temperature (400-600 °C). It might be the main reason of relatively high CH_4 selectivity of CeO_2 at high temperature.

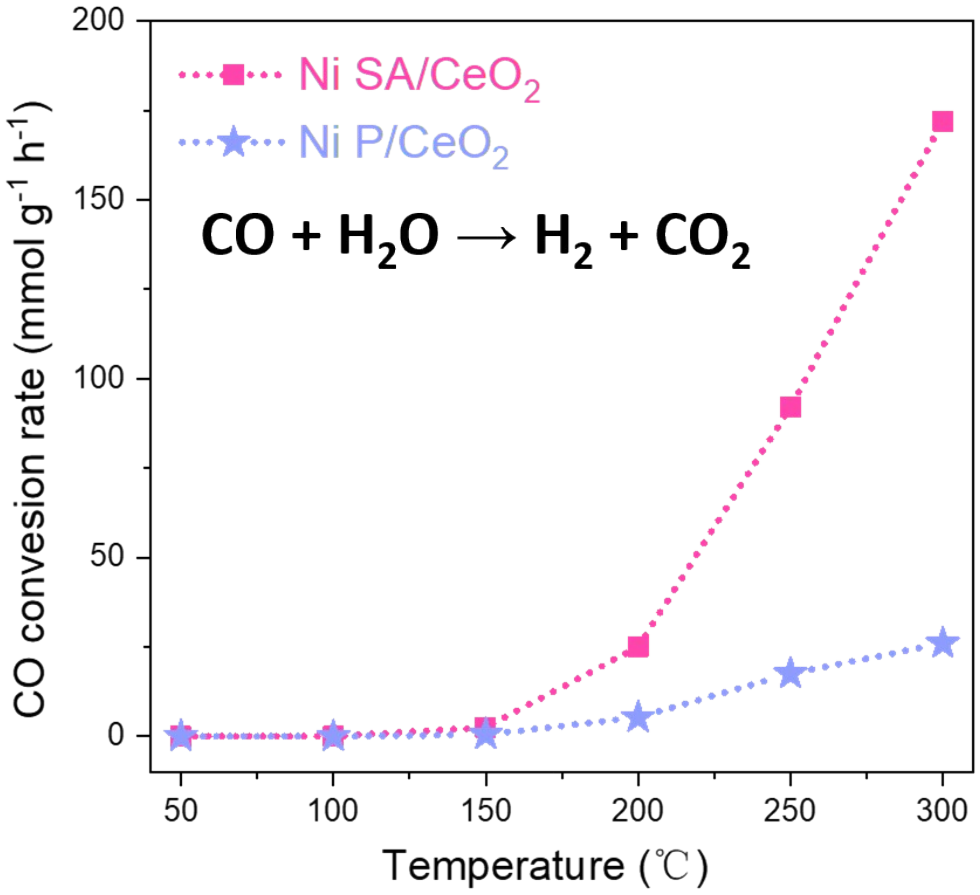

Figure S14. The CO steam reforming performance over Ni SA/CeO_2 and Ni P/CeO_2.

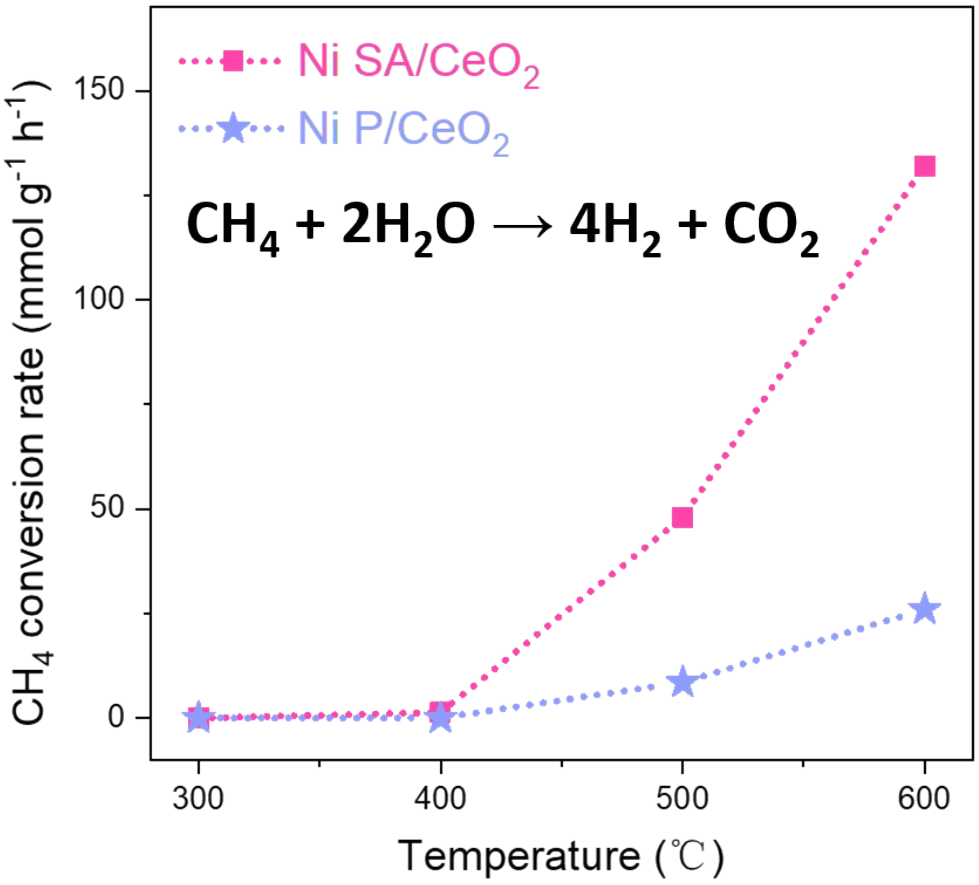

Figure S15. The CH_4 steam reforming performance over Ni SA/CeO_2 and Ni P/CeO_2.

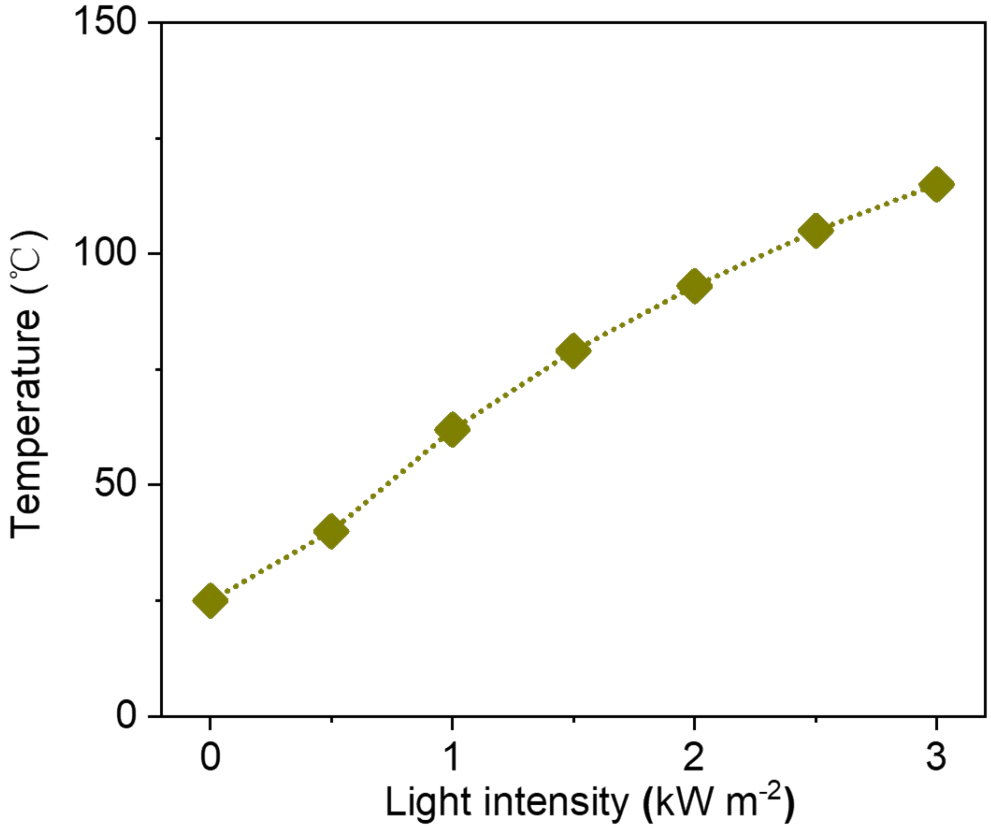

Figure S16. The temperature of Ni SA/CeO_2 direct under different intensities of solar irradiation.

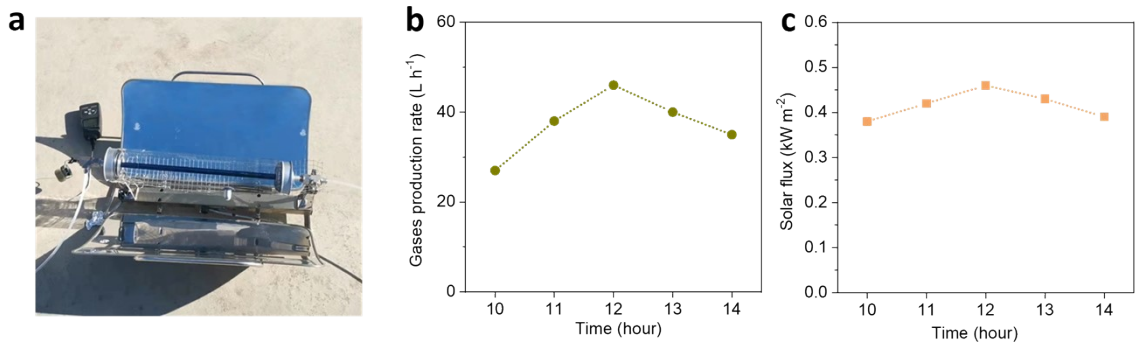

Figure S17. (a) Optical image of the outdoor solar-heating ESR system. (b, c) The ESR gases production rate and solar flux as a function of time under ambient sunlight irradiation on December 14, 2021, in the Baoding city, China.

References

1. Y. Li, J. Hao, H. Song, F. Zhang, X. Bai, X. Meng, H. Zhang, S. Wang, Y. Hu and J. Ye, *Nature Communications*, 2019, **10**, 2359.
2. G. Kresse and J. Furthmüller, *Computational Materials Science*, 1996, **6**, 15-50.
3. G. Kresse and J. Furthmüller, *Physical Review B*, 1996, **54**, 11169-11186.
4. J. P. Perdew, K. Burke and M. Ernzerhof, *Physical Review Letters*, 1996, **77**, 3865-3868.
5. G. Kresse and D. Joubert, *Physical Review B*, 1999, **59**, 1758-1775.
6. P. E. Blöchl, *Physical Review B*, 1994, **50**, 17953-17979.
7. S. Grimme, J. Antony, S. Ehrlich and H. Krieg, *The Journal of Chemical Physics*, 2010, **132**, 154104.
8. O. S. Popel and A. B. Tarasenko, *Thermal Engineering*, 2021, **68**, 807-825.